scientific reports

OPEN

Experimental and first-principles investigation on how support morphology determines the performance of the Ziegler-Natta catalyst during ethylene polymerization

Tinnakorn Saelee[1,2,3,7], Pichayapong Sitthijun[2,7], Chinanang Ngamlaor[1,2], Nuttapat Kerdprasit[1,2], Meena Rittiruam[1,2,4], Patcharaporn Khajondetchairit[1,2,5], Juarez L. F. Da Silva[6], Nichakorn Buasuk[1,2], Piyasan Praserthdam[2] & Supareak Praserthdam[1,2]✉

One class of the Ziegler–Natta catalysts (ZNC) – the $TiCl_4$/$MgCl_2$ having triethyl aluminum ($AlEt_3$), has been widely utilized during ethylene polymerization. Although the Ti species plays the role of a major active site, an increase of Ti species does not always improve the activity of ZNC. Herein, investigations of experiments and density functional theory (DFT) elucidate this inverse effect of the increased amount of $TiCl_4$ deposition in ZNC because of the pretreatment process. However, the activity of ZNC on pretreated $MgCl_2$ dropped to 60% of the unpretreated one. The DFT demonstrates that the pretreatment strengthened the interaction between $TiCl_4$ and ZNC, especially on the (104) surface, forming the $TiCl_4$-$TiCl_4$ cluster. The existence of this $TiCl_4$-$TiCl_4$ cluster found on the ZNC (104) surface weakens the adsorption of the first $AlEt_3$ molecule and obstructs further alkylation process, making another Ti site of the alkylated $TiCl_4$-$TiCl_4$ cluster inactive. However, the difficult formation of the TiCl4-TiCl4 cluster found on the ZNC (110) is an important key point that enables the activation of all adsorbed $TiCl_4$ on this surface by facilitating the alkylation process. Moreover, the existence of the $MgCl_2$ (110) surface prevents the formation of the $TiCl_4$-$TiCl_4$ cluster significantly. Hence, it is suggested that the existence of the (110) plane on ZNC plays a key role in controlling the performance of the ZNC, especially the stability via the prevention of deactivation caused by the clustering of $TiCl_4$.

Keywords Ziegler–Natta, Catalyst deactivation, First-principles, Density functional theory, $TiCl_4$ cluster

Ziegler–Natta catalyst (ZNC) has been conventionally used in petrochemical industries for the production of polymeric material, i.e., polyethylene, polyolefin[1,2], and polypropylene[3–6], where the two common types of ZNC used are titanium- and vanadium-based[7,8]. Since the 1950s, the fourth generation of ZNC has been based on titanium tetrachloride ($TiCl_4$) on magnesium chloride ($MgCl_2$) support. Moreover, alkyl aluminum, which is an organoaluminium compound, was also added as a co-catalyst[9]. Regarding the procedure, the alkylation process can reduce the Ti^{4+} species of the chloride ligand to form the active species of Ti^{3+} and Ti^{2+}. The reduced Ti species are crucial for the formation of a complex surrounded by ethylene molecules[10,11]. Moreover, it is worth noting that the Ti^{2+} species was also found to be the active center for ethylene polymerization[12–15]. One of many

[1]High-Performance Computing Unit (CECC-HCU), Center of Excellence on Catalysis and Catalytic Reaction Engineering (CECC), Faculty of Engineering, Chulalongkorn University, Bangkok 10330, Thailand. [2]Center of Excellence on Catalysis and Catalytic Reaction Engineering (CECC), Faculty of Engineering, Chulalongkorn University, Bangkok 10330, Thailand. [3]Saelee Research Group, Bangkok 10330, Thailand. [4]Rittiruam Research Group, Bangkok 10330, Thailand. [5]Khajondetchairit Research Group, Bangkok 10330, Thailand. [6]São Carlos Institute of Chemistry, University of São Paulo, P.O. Box 780, São Carlos, SP 13560-970, Brazil. [7]These authors contributed equally: Tinnakorn Saelee and Pichayapong Sitthijun. ✉email: supareak.p@chula.ac.th

upgrading methods for improving the performance of ZNC is the enhancement of the $TiCl_4$ loading, in which the pretreatment process can significantly promote the amount of $TiCl_4$ deposition on the $MgCl_2$ surface[16–20].

Although the amount of $TiCl_4$ can be increased, it does not confirm that all added $TiCl_4$ can be activated as the active Ti species. Hence, understanding the mechanism of ZNC formation, including (1) the titanation process, which introduces the $TiCl_4$ on the $MgCl_2$ support, and (2) the alkylation process, in which the alkyl aluminum interacts with the adsorbed $TiCl_4$ species, is crucial and need to unravel. To do so, the density functional theory (DFT) is an effective tool that can elucidate the insight information of the thermodynamically stable structure and the electronic charge properties for describing what phenomena have probably undergone during the titanation and alkylation processes. Taniike et al[21]. employed the DFT calculation to define the coordination modes of titanium and other donors on the $MgCl_2$ surface of $MgCl_2/TiCl_4/ID/AlR_3/ED$ in which the most stable structures of $MgCl_2/TiCl_4/ID/AlR_3/ED$ were illustrated. Zorve and Linnolahti[22]. computationally investigated the adsorption of $TiCl_4$ on $MgCl_2(104)$ and $MgCl_2(110)$ surfaces to describe that the mononuclear $TiCl_4$ prefers to adsorb at the defect site of $MgCl_2(110)$ surface by creating the six-coordination bond formation. On the one hand, the resemblance of a binuclear of Ti_2Cl_8 can be found on the $MgCl_2(104)$ surface, shedding light on how the active centers are presented. Cheng et al.[23].computationally investigated the sequence of electron donors via twelve possible ZNC models, including mono-nuclear and di-nuclear $TiCl_4$. Moreover, the effect of ethyl benzoate (EB), which is the electron donor, on perfect and defective $MgCl_2(110)$ and $MgCl_2(100)$. They found that the EB molecule prefers to adsorb on the support over the $TiCl_4$ region, obstructing the coordination of $TiCl_4$ on the $MgCl_2$ surfaces.

Herein, the combined experiment and DFT calculation in which the experimental observation found some important phenomena of catalytic deactivation during the ethylene polymerization process. Meanwhile, the DFT calculation is cooperated to describe the deactivation's cause. The results obtained via this work can be used to design a better ZNC.

Results and discussion

Experimental results

Morphological properties

The effect of the pretreatment process on morphological changes of ZNC was primarily investigated via SEM analysis. The SEM images are shown in Fig. 1, while the average particle size of the catalyst and the amount of deposited Ti in ZNC bulk, measured by ICP, are summarized in Table 1. Overall, the physical appearances of unpretreated and pretreated ZNCs are not significantly different. Moreover, the average particle sizes of unpretreated ZNC (around 21 μm) and pretreated ZNC (around 36 μm) in this work are in the ranges of conventional

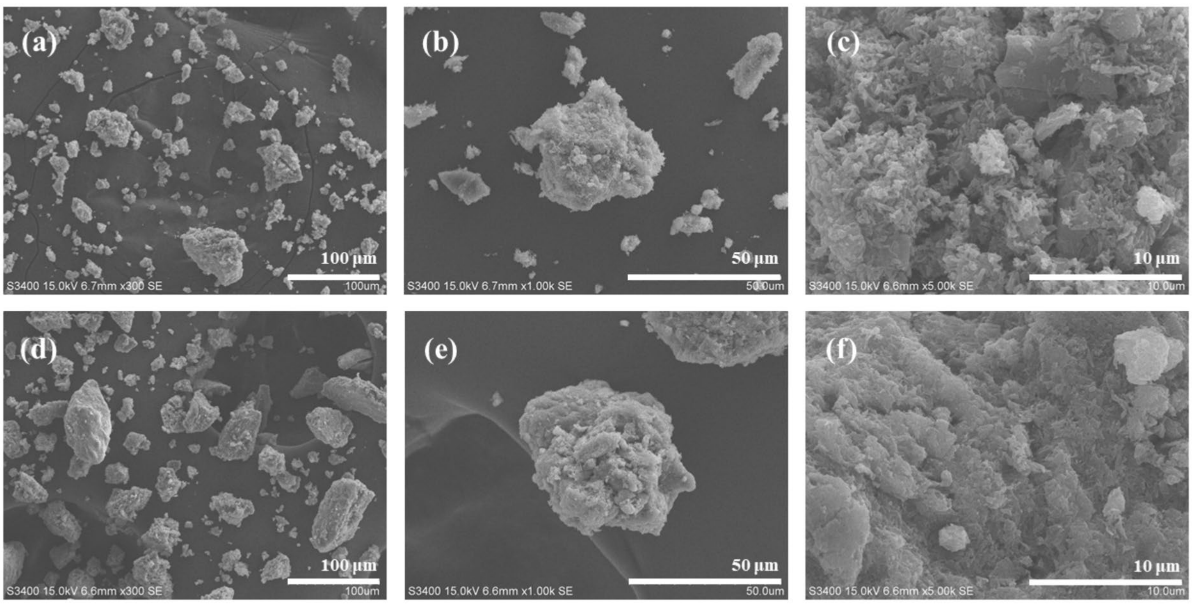

Figure 1. SEM images of (**a**)-(**c**) unpretreated and (**d**)-(**f**) pretreated ZNC.

Catalyst	Ti content[a] (wt%)	Average size[b] (μm)
Unpretreated ZNC	4.6	~21
Pretreated ZNC	10.1	~36

Table 1. Amount of Ti content and average particle size of ZNCs. [a]Ti content in the bulk catalyst was detected by ICP. [b]Average size of the catalyst was measured by SEM detector.

ZNC (20 to 40 μm)[24]. Intriguingly, The 4.6 wt% of Ti species in unpretreated ZNC and 10.1 wt.% of pretreated ZNC indicates that the pretreating process can increase the amount of Ti deposition during titanation process, suggesting that the interaction between the $MgCl_2$ surface and $TiCl_4$ is significantly improved[20,25].

In order to elucidate the distribution of $TiCl_4$ species, especially on the surface of unpretreated and pretreated ZNCs, the elemental analysis via EDX spectroscopy was performed, as shown in Fig. 2. The blue and red dots in the EDX mapping represent the elemental distribution of Ti and Mg species, respectively. It is found that the dispersions of Ti and Mg species on both unpretreated and pretreated ZNCs seem uniform. However, the Ti species on the pretreated ZNC is more condensed, while the density of Mg species on both ZNCs is comparable. Furthermore, the molar ratios of Ti/Mg on unpretreated and pretreated ZNCs are 0.3 and 1.8, respectively. The higher amount of Ti/Mg ratio found on the pretreated ZNC reveals that performing the pretreatment process successively increases the amount of the Ti species deposition in both bulk structures, elucidated by ICP, and the catalyst surface, distinguished by SEM–EDX.

The crystallinity of $MgCl_2$ support during the titanation process

Regarding the previous section that clearly proves that pretreatment of $MgCl_2$ can increase the amount of TiCl4 loading on the ZNC surface, the crystallinity of ZNC is another crucial factor that has to be investigated in order to confirm phase transformation of ZNC that normally takes place during the titration process[26,27]. Herein, the XRD patterns of clean $MgCl_2$ support and ZNCs are illustrated in Fig. 3, showing sharp peaks at 2θ of 15°, 30°, 35°, and 50° corresponding to the Miller index of (003), (102), (104), and (110), respectively. These characteristic peaks refer to the unique character of $MgCl_2$ in the alpha phase (α-$MgCl_2$)[20,28]. After the titanation process, all mentioned peaks invincibly disappear. These results demonstrate the scenario of the phase transformation in which the α-$MgCl_2$ undergoes the delta phase of $MgCl_2$ (δ-$MgCl_2$). Nevertheless, the δ-$MgCl_2$ is realized as mainly an amorphous phase[27]. Hence, the crystal peak on the XRD patterns of both unpretreated and pretreated ZNCs does not clearly exhibit.

Regarding the δ-$MgCl_2$, three facets; including (001), (104), and (110) planes, are normally considered[29,30]. Among them, only (104) and (110) facets significantly influence the titanation process. On the other hand, the presence of an inactive Mg center found in the δ-$MgCl_2$(001) surface makes the (001) facet inactive for the titanation process. Hence, investigation on the ZNC, especially on the δ-$MgCl_2$(001) surface, can be neglected, as discussed in various works[28,31].

In this work, small amplitudes of ~ 32° and ~ 50° representing (104) (marked as a star) and (110) (marked as a triangle) facets of δ-$MgCl_2$ support[20,28] are observed. However, these signals are not strong enough to explain which facet is dominant. Therefore, consideration of the catalytic performance of ZNCs via $MgCl_2$(104) and δ-$MgCl_2$(110) surfaces is selected. According to these strategies, theoretical investigation via the ZNC(104) and ZNC(110) models was performed and discussed in the computational section.

The activity of ZNCs during ethylene polymerization

As mentioned, the pretreatment process can add $TiCl_4$ species, which can further activate during the alkylation process. The $TiCl_4$ species which is interacted with the $AlEt_3$ reduces Ti species. Then, the reduced Ti species

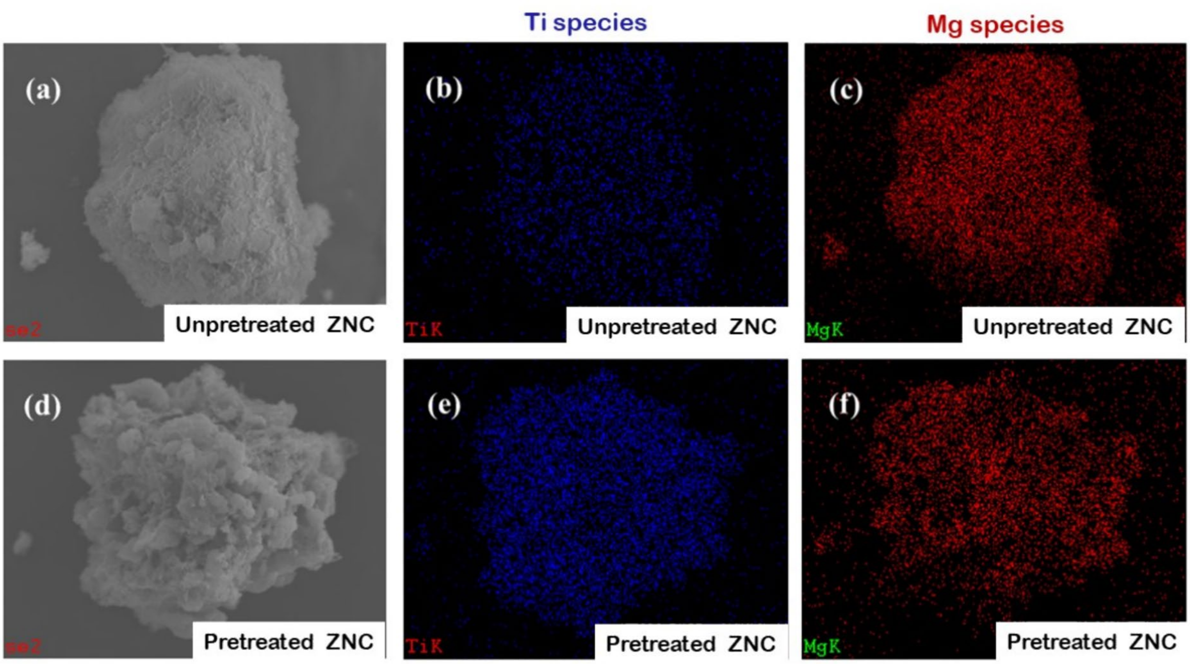

Figure 2. The SEM–EDX image representing a distribution of Ti species (blue spot) and Mg species (red spot) on (**a**-**c**) unpretreated and (**d**-**f**) pretreated ZNCs.

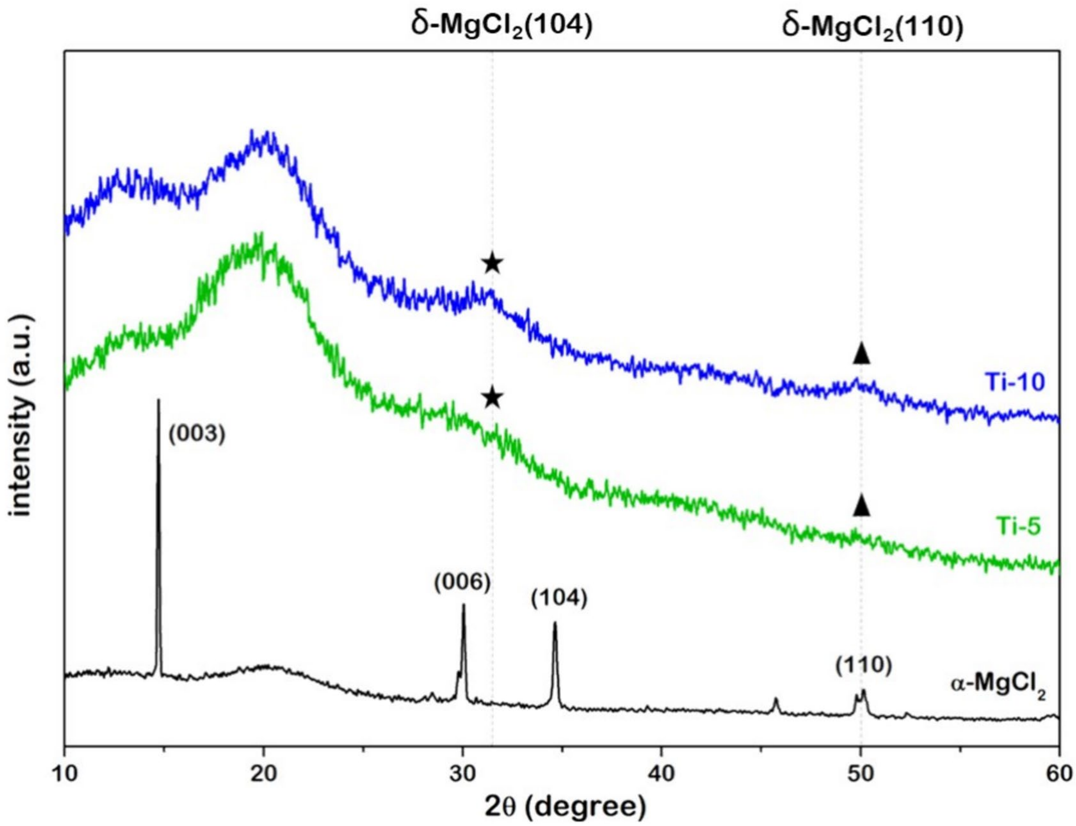

Figure 3. The XRD patterns of clean α-$MgCl_2$ (black) before the titanation process, unpretreated (green), and pretreated (blue) ZNCs containing $TiCl_4$ on $MgCl_2$ support.

can attack the π electron of ethylene monomer at the initial state of ethylene polymerization[32,33]. In this work, the concentration of $AlEt_3$ was varied. The ratios of Al/Ti are listed in Table 2. Moreover, the normalized catalytic activity in the function of the Al/Ti ratio is plotted in Fig. 4, in which the activity plot can be classified by two main states. For the first state, the activity of ZNC for ethylene polymerization is increased as the function of $AlEt_3$, in which the optimum Al/Ti ratios refer to the maximum catalytic activity. The optimum Al/Ti of unpretreated and pretreated ZNCs are 120 and 140, respectively. The lower optimum value of the Al/Ti ratio on unpretreated ZNC reflects that unpretreated ZNC consumes less amount of Al to activate the Ti species. These results also confirm that the amount of Ti species, which is possible to be activated, on the unpretreated ZNC is less than that on the pretreated ZNC.

After the optimum point, the second state takes place. The catalytic activity is significantly declined according to the function of $AlEt_3$ loading. These results reflect the overloading of $AlEt_3$ after the optimum Al/Ti ratio, inducing the over-reduction of Ti species from Ti^{+4} to Ti^{+}, in which this Ti^{+} species is inactive for ethylene polymerization[34,35]. Interestingly, consideration of the absolute activities of unpretreated and pretreated ZNCs elucidates that the absolute activities of ethylene polymerization on unpretreated ZNC are approximately two times higher than that on the pretreated one in every Al/Ti ratio even though the amount of deposited Ti species on pretreated ZNC is higher. According to these results, there is a crucial clue as to why the increment of the Ti

	Unpretreated ZNC		Pretreated ZNC	
Al/Ti molar ratio	Activity^a	Relative activity	Activity^a	Relative activity
80	1047.43	0.45	553.48	0.58
110	2040.69	0.89	719.16	0.75
120	2305.06	1.00	770.52	0.81
140	2230.67	0.97	952.60	1.00
170	1885.71	0.82	798.27	0.84
200	1262.78	0.55	157.23	0.17

Table 2. The activity of ethylene polymerization in various Al/Ti ratios. ^{a}Catalytic activity unit is $kgPE.molTi^{-1}.h^{-1}$.

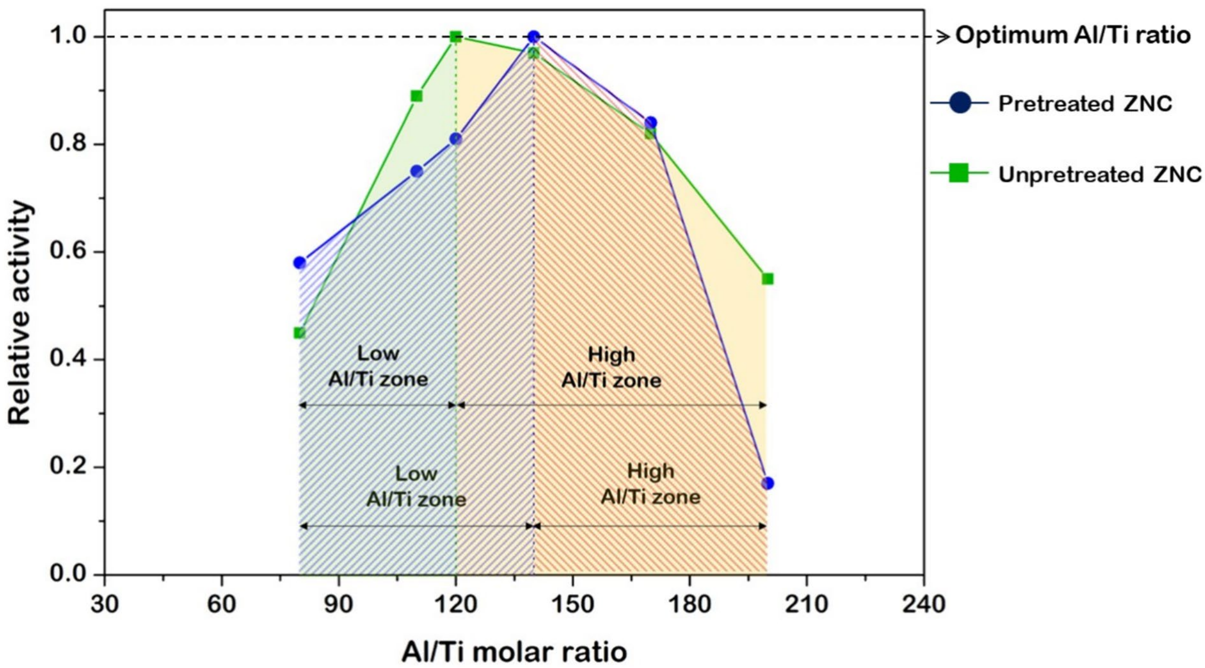

Figure 4. The plots of relative activity in the function of the Al/Ti molar ratio of unpretreated (green) and pretreated (blue) ZNCs.

content decreases the catalytic activity for ethylene polymerization. To answer this question, DFT participated in the computational section.

Computational results

Adsorption of $TiCl_4$ on $MgCl_2(104)$ and $MgCl_2(110)$ surfaces

According to the experimental observation, phase transformation of the α-$MgCl_2$ to the δ-$MgCl_2$ was observed during titanation process in which the structure of δ-$MgCl_2$ probed via XRD revealed equivocal judgment on either (104) or (110) facet is dominant. Hence, the construction of both (104) and (110) surfaces was not ignored. The scenario of two concentrations of $TiCl_4$ on δ-$MgCl_2$(104) and δ-$MgCl_2$(110) surfaces was scoped to represent low-concentration (L104 and L110) and high-concentration (H104 and H110) models. The most stable geometries of L104, L110, H104, and H110 are illustrated in Fig. 5. It is noted that the single molecular $TiCl_4$ adsorption represents L104 and L110, while the bimolecular $TiCl_4$ adsorption represents H104 and H110. Also, adsorption energy (E_{ads}), the contact point between each bonding atom, and the adsorption height of each adsorbate are included in Table 3. All possible optimized geometries are shown in Table S1 in the supplementary document.

For the (104) plane, the single molecule of $TiCl_4$ can be adsorbed with the E_{ads} of −0.53 eV by creating three contact points: Cl1-Mg1, Cl2-Mg2, and Ti1-Cl5. In the case of bimolecular adsorption of $TiCl_4$ on δ-$MgCl_2$(104) surface, the interaction of the second $TiCl_4$ molecule is strengthened in which the E_{ads} is −0.73 eV. The two additional contact points of Cl4-Mg3 and Ti2-Cl6 are created. The more negative E_{ads} during the second $TiCl_4$ adsorption implies the promotional effect of the first $TiCl_4$ molecule enhancing $TiCl_4$ adsorption. These results agree well with the experimental observation that the existence of $TiCl_4$ species from the pretreatment process can facilitate more amount of $TiCl_4$ adsorption in the upcoming impregnation process[25]. However, adsorption of the new coming $TiCl_4$ on H (104) seems to occur of $TiCl_4$ clustering on the δ-$MgCl_2$ (104) surface.

For the (110) plane, the single molecule of $TiCl_4$ can be adsorbed with the E_{ads} of −1.05 eV by creating the four contact points of Cl1-Mg1, Cl2-Mg2, Ti1-Cl5, and Ti1-Cl6. The most favorable adsorption site is elucidated at the defect site of the δ-$MgCl_2$ (110) surface. The more negative E_{ads} compared to that on the δ-$MgCl_2$ (104) surface reveals that the interaction of TiCl4 on the δ-$MgCl_2$ (110) surface is stronger than that on the δ-$MgCl_2$ (104) surface because the presence of the defective site facilitates the creation of four contact points between $TiCl_4$ and δ-$MgCl_2$ (110) surface. Thereby, the appearance of the "defect" site is one of the most important key roles in improving $TiCl_4$ deposition on $MgCl_2$ support. When the concentration of $TiCl_4$ on the δ-$MgCl_2$ (110) surface is increased, the second $TiCl_4$ molecule is adsorbed on the second defective site of the δ-$MgCl_2$ (110) surface in which the E_{ads} of the second molecule of $TiCl_4$ is comparable to the single molecular $TiCl_4$ adsorption. According to these results, the dispersion of the defective site on the δ-$MgCl_2$ (110) surface is a key factor in controlling the distribution of deposited $TiCl_4$ in which control of the distribution of the $TiCl_4$ on δ-$MgCl_2$ (104) is more difficult.

Alkylation of $TiCl_4$ species on H104 and H110 surfaces

To activate the deposited $TiCl_4$ readily for ethylene polymerization, the alkylation process must be first performed when the addition of the $AlEt_3$ is introduced. Regarding the experimental question, why does an increment of $TiCl_4$ deposition deteriorate the catalytic activity for ethylene polymerization? Consideration of the geometries

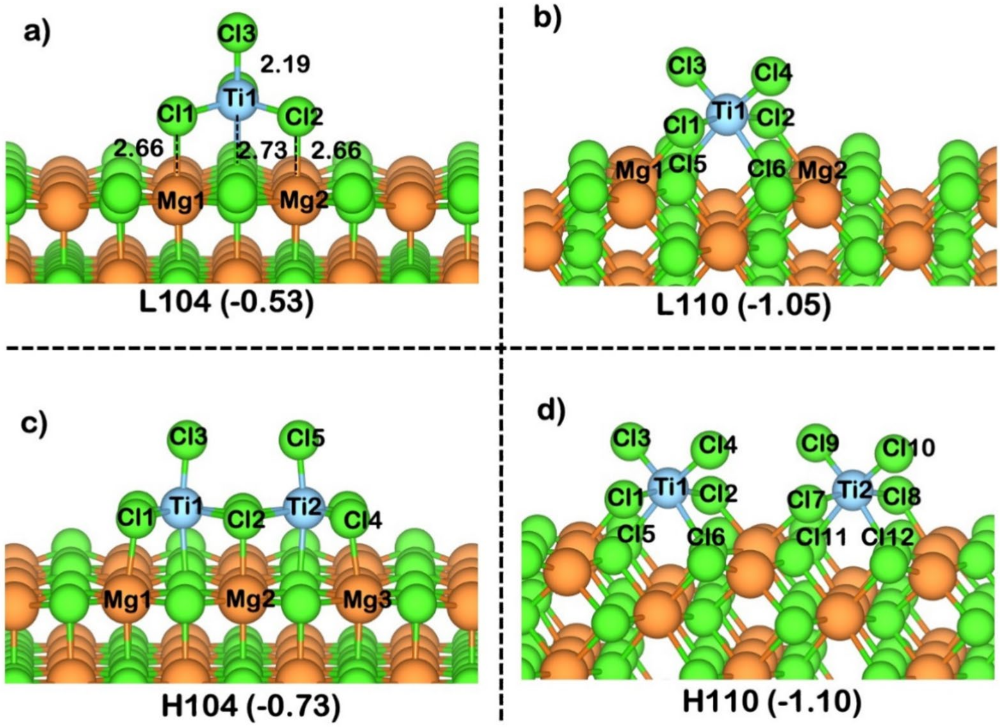

Figure 5. Stable geometries of (**a**) L104, (**b**)L110, (**c**) H104, and (**d**) H110 surfaces.

Structure	E_{ads} (eV)	Contact point	Adsorption height (Å)
L-104	−0.53	Cl1-Mg1, Cl2-Mg2, Ti1-Cl5	2.66
L-110	−1.05	Cl1-Mg1, Cl2-Mg2, Ti1-Cl5 Ti1-Cl6	2.46
H-104	−0.73	Cl1-Mg1, Cl2-Mg2, Cl4-Mg3 Ti1-Cl5, Ti2-Cl6	2.54
H-110	−1.10	Cl1-Mg1, Cl2-Mg2, Ti1-Cl5 Ti1-Cl6, Cl7-Mg2, Cl8-Mg3, Ti2-Cl11, Ti2-Cl2	2.46

Table 3. Adsorption energies (E_{ads}) in eV, contact points of $TiCl_4$ on MgCl2(10_4) and $MgCl_2$ (110) surfaces, and adsorption height in Å of $TiCl_4$, including single $TiCl_4$ molecule and $TiCl_4$ cluster on MgCl2(104) and (110) surfaces.

of ZNCs, especially the high $TiCl_4$ contents, including H104 and H110, when interacting with the $AlEt_3$, is performed. From various possible adsorbed configurations of $AlEt_3$, as listed in Table S2, the most stable geometries of each $AlEt_3$-H104 and $AlEt_3$-H110 are demonstrated in Fig. 6a and Fig. 6b. Furthermore, the electron density difference (EDD), which is depicted as the contour plot, together with Bader charge analysis values, are expressed in Fig. 6c and Fig. 6d.

The red region corresponds to the negative Bader charge value representing electron accumulation. In contrast, the blue region with the positive Bader charge refers to electron depletion. For the alkylation on the H104 surface, the $AlEt_3$ prefers to adsorb on $TiCl_4$ by creating the interaction of Al-Cl3 with the E_{ads} of −0.47 eV and the adsorption height of 2.54 Å. For alkylation of the H110 surface, adsorption of $AlEt_3$ takes place via the connection of the Al species of $AlEt_3$ to the Cl4 species of the adsorbed $TiCl_4$ with an E_{ads} of −0.58 eV and the adsorption height of 2.46 Å.

The appearance of a negative Bader charge of the adsorbed $AlEt_3$ species corresponding to the positive Bader charge of surfaces, including H104 and H110 surfaces, elucidates the scenario of electron transfer from catalyst surfaces to adsorbed $AlEt_3$ molecule. Moreover, the less negative Bader charge of the $AlEt_3$ molecule on the H104 surface compared to the H110 surface agrees well with the weaker interaction of $AlEt_3$ on the H104 surface.

Intriguingly, the change of Bader charge of Ti1 species during the formation of H104 higher $TiCl_4$ and adsorption of $AlEt_3$ demonstrate sharing electron around the first and second $TiCl_4$ molecule on only ZNC (104) surface due to agglomeration of $TiCl_4$. Focusing on the Bader charge of the Ti1 species in L104 (denoted as + 0.46 |e|) and H104 (denoted as −0.29 |e|), which is reported in Table S3, changing of the Bader charge when the formation of the $TiCl_4$-$TiCl_4$ cluster exhibits that there is electron transfer between the first species of $TiCl_4$ and the second species of $TiCl_4$. These results elucidate that there is an interaction between two $TiCl_4$ species, confirming the clustering of $TiCl_4$-$TiCl_4$ on H104. This agglomeration is not observed during the transformation of L110 to H110.

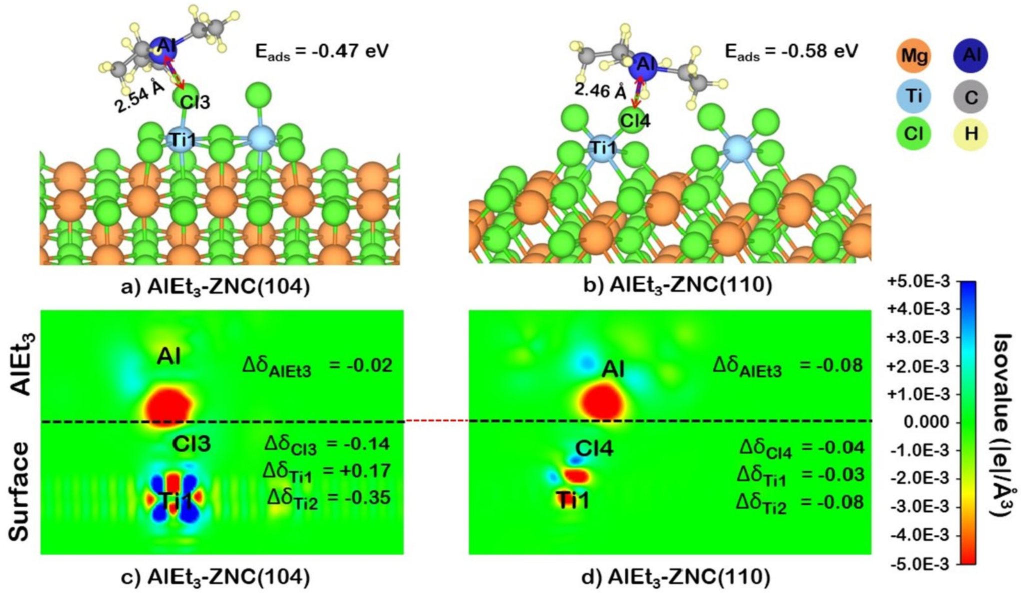

Figure 6. The geometries of $AlEt_3$ adsorption on (**a**) ZNC(104) and (**b**) ZNC(110).

The presence of $TiCl_4$-$TiCl_4$ cluster has negative effects, not only weakening the interaction between $AlEt_3$ and deposited $TiCl_4$ but the presence of $TiCl_4$-$TiCl_4$ cluster prevents dispersion of $TiCl_4$, making only one species of $TiCl_4$-$TiCl_4$ cluster can be activated via interacting with the first $AlEt_3$ whereas the other is still inactive because of the steric hindrance of the adsorbed $AlEt_3$ hindering the further alkylation process. As a result, there is only one active species readily available for ethylene polymerization. On the other hand, the good dispersion of TiCl4 species supports activation of the adsorbed $TiCl_4$ species in the upcoming alkylation process because the good distribution of $TiCl_4$ species on the special defective site overcomes the steric effect of $AlEt_3$. Thereby, the activity of the H110 is possibly higher than that of H104. The results obtained by DFT calculation suggest that the increment of TiCl4 loading does not always enhance the activity of ZNC, but the increment of the TiCl4 contents on the (110) plane of ZNC is more important in enhancing the performance of the ZNC. In contrast, an increment of $TiCl_4$ deposition on the (104) plane of ZNC promotes the enlargement of the $TiCl_4$-$TiCl_4$ cluster, lowering the activity of ZNC.

Conclusion

The issue of how the $MgCl_2$ support pretreatment improves the amount of $TiCl_4$ deposition on the ZNC catalyst yields a low-performance ZNC is investigated. Overall, the phase transformation from α-$MgCl_2$ to δ-$MgCl_2$ was observed during the titanation process. Also, the δ-$MgCl_2$ (104) and δ-$MgCl_2$ (110) are dominant surfaces. Although the pretreatment process can increase the amount of $TiCl_4$ loading, the absolute catalytic activity for the unpretreated ZNC is still higher. The DFT calculation participated in unraveling why the higher content of TiCl4 deposition lowering deactivated the ZNC. It is demonstrated that the pretreatment process could enhance the adsorption of further $TiCl_4$ species, but the clustering of $TiCl_4$-$TiCl_4$ cluster, especially on the H104 surface, is also easily facilitated. However, the presence of a $TiCl_4$-$TiCl_4$ cluster is not observed on the H110 surface. The presence of the $TiCl_4$-$TiCl_4$ cluster has a negative effect in terms of blocking the second alkylation process, whereas the first alkylation process can be done normally. Hence, only one $TiCl_4$ species can be activated even though two $TiCl_4$ were introduced. On the other hand, two species of $TiCl_4$ on H110 can be fully activated via the alkylation process. The results obtained by DFT calculation suggest that the key point for enhancing the activity in ZNC is not always the amount of $TiCl_4$ loading but controlling either the presence of $MgCl_2$(110) or other special support that can prevent the formation of the TiCl4-TiCl4 cluster is more crucial for improving the performance of a better ZNC.

Methodology

Experimental details

Catalyst preparation

All preparations were carried out under the purified N_2 atmosphere (supplied by Linde (Thailand) Ltd.). Firstly, the $MgCl_2$ mixture was produced. The 2 g of anhydrous $MgCl_2$ (purchased from Merck Ltd.) were suspended in 150 mL of n-heptane. Then, 12.30 mL of ethanol (EtOH) was added. This process is called the EtOH adduct process[26,36,37]. Subsequently, the mixture was homogenized at 120 ℃ for 2 h under a continuously refluxed condition. This precursor is indispensable for synthesizing ZNC in the upcoming step.

The two types of ZNCs, including (1) unpretreated and (2) pretreated ZNCs, were synthesized. For the unpretreated ZNC, the 11.50 mL of $TiCl_4$, which was dissolved in 1 M of toluene, was added to 40 ℃ of the $MgCl_2$ mixture. The titanation process was carried out by introducing the $TiCl_4$ into the $MgCl_2$ mixture, in which the molar ratio of Ti and Mg was controlled at 5:1. For the pretreated ZNC, the 2.30 mL of $TiCl_4$ solution was firstly introduced into the $MgCl_2$ mixture to pretreat the $MgCl_2$ surface in order to dealcoholize the $MgCl_2$.nEtOH adduct in which the equivalent molar ratio of Ti and Mg species was regulated. After that, the $TiCl_4$ solution was introduced again to the dealcoholized $MgCl_2$ through the same condition as the unpretreated ZNC.

When the titanation process was complete, all unpretreated and pretreated ZNCs were continually heated at 120 °C for 2 h before cooling down to room temperature. Finally, pretreated and unpretreated ZNCs were washed several times with the distilled hexane in order to eliminate impurities and excess $TiCl_4$ before drying at 110 ℃ under a vacuum overnight. The dried ZNCs were safely stored under an Ar atmosphere.

Characterizations

The Ti content in each ZNC sample was measured via the inductively coupled plasma atomic emission spectroscopy (ICP-AES) by Perkin Elmer equipped with a 2100-DV inductively coupled plasma (ICP). The 0.01 g of each catalyst were dissolved in 5 mL of hydrochloric acid before being diluted with 100 mL of deionized water. The morphology and particle size were revealed through the secondary electron detector of scanning electron microscopy (SEM) performed on a Hitachi-S3400N model. In addition, the elemental analysis of Ti and Mg on ZNC was determined by the energy-dispersive X-ray spectroscopy (EDX) on the Apollo X model with the Edex 2371 series. Moreover, the crystallinity and phase transformation of $MgCl_2$ support before and after the titanation process were analyzed by the powder X-ray diffraction (XRD), Bruker D8 Advance, with a diffraction angle (2θ) of 10° to 60°. The scanning speed was set as 0.5 s/step.

Polymerization reaction testing

The 0.01 g of ZNC was introduced into a stainless-steel autoclave reactor. Then, the $AlEt_3$ cocatalyst (donated by Thai Polyethylene Co. Ltd.) was added to the reactor. The hexane was then injected until the final volume reached 30 mL (note that the concentrations of $AlEt_3$ were varied in which the molar ratio of Al:Ti was set as 80:1, 110:1, 120:1, 140:1, 170:1, and 200:1). When all components were added, the reactor was vacuumed by evacuating the under vacuum condition for 10 min. The reaction was begun by ramping the temperature up to 70 ℃ in a heated water bath. Then, the reactor was soaked in the water bath. When the temperature was at equilibrium. The slurry polymerization of ethylene was taken place by feeding 7 bars of ethylene gas into the reactor continuously for 10 min. The reaction was terminated by (1) cooling the system down to room temperature and (2) adding 3.0 M of hydrochloric acid dissolved in methanol in order to precipitate the produced polymer. Finally, the solid phase samples, including ZNC and precipitated polymer, were washed using purified ethanol before drying at 110 ℃ until the weight became stable. The catalytic activity and relative activity are calculated in Eq. 1 and Eq. 2, respectively.

$$\text{Catalytic activity} = \frac{\text{obtained PE polymer(kg)}}{(\text{Ti in the catalyst (mol)}) \times (\text{Reaction time (s)})} \tag{1}$$

$$\text{Relative activity} = \frac{\text{Catalytic activity}}{\text{Maximum activity}} \tag{2}$$

Computational details

Catalyst modeling and parameters

All stable geometries and electronic properties were performed using DFT calculation, which was implemented through the Vienna ab initio simulation package (VASP 5.4.4)[38–41]. The projector augmented wave (PAW) of the generalized gradient approximation (GGA) proposed by Perdew, Burke, and Ernzerhof (PBE) functional was employed in the calculation[42]. The structural optimization was performed through the conjugate gradient method[43] until the energy convergence was lower than 10^{-6} eV and the force convergence was less than 0.01 eV/Å. Moreover, the Van der Waals dispersion force is considered by applying the DFT–D3 method proposed by Grimme et al.[44] During the optimization, the 3 × 3 × 1 Monkhorst–Pack *k*-mesh Brillouin-zone integration[45] was used. The VESTA package[46] was used to visualize all models. The interaction between the catalyst surface and the adsorbed molecule was characterized by the adsorption energy (E_{ads}) calculated by Eq. 3.

$$\Delta E_{ads} = \Delta E_{complex} - \Delta E_{adsorbent} + \Delta E_{adsorbate} \tag{3}$$

The parameters: $\Delta E_{complex}$, $\Delta E_{adsorbent}$, and $\Delta E_{adsorbate}$ are the calculated energies of the complex system (molecule-adsorbed surface), clean surface and adsorbed molecule ($TiCl_4$ as well as $AlEt_3$ species) are considered. The partial charge accumulation or depletion during the adsorption process ($\Delta\rho_{ads}$) of $AlEt_3$ on $TiCl_4/MgCl_2$ catalyst was calculated based on the Bader charge analysis[47–50] defined in Eq. 4.

$$\rho_{ads} = \rho_{surface\text{ - }TEA} - \rho_{surface} - \rho_{AlEt_3} \tag{4}$$

The parameters: $\rho_{surface\text{ - }TEA}$, $\rho_{surface}$, and $\rho_{surface\text{ - }TEA}$ denote partial charge densities of adsorbed surface, catalyst surface, and an isolated molecule, respectively. The geometry of an isolated molecule (either $TiCl_4$ or $AlEt_3$) and the clean $MgCl_2$ supports were constructed, as shown in Fig. 7. The stable $MgCl_2$ surfaces of (110) and (104), including their possible active sites, are shown in Fig. 7a,b), respectively. Also, the four atomic layers of $MgCl_2$(110) and $MgCl_2$(104) surfaces were constructed.

Interaction between the periodic boundary was avoided by adding ~ 20 Å vacuum region along the z-axis of the slab model. All possible adsorption sites include (1) atop the site of Mg (A-Mg), (2) atop the site of Cl (A-Cl),

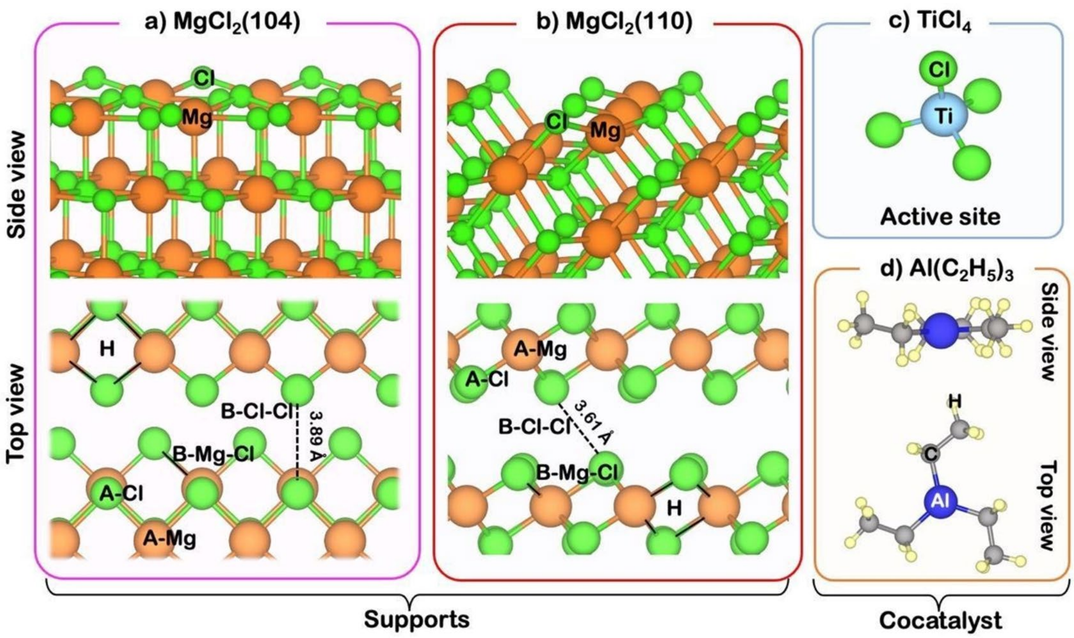

Figure 7. Structural geometries of (**a**) $MgCl_2$(104), (**b**) $MgCl_2$(110) with their possible adsorption sites, (**c**) $TiCl_4$, and (**d**) $AlEt_3$.

(3) bridge between Cl and Cl (B-Cl-Cl), (4) bridge site between Mg and Cl (B-Mg-Cl), and (5) the hollow site (H). During optimization, the bottom two layers of $MgCl_2$ surfaces were fixed to their bulk lattice parameter, while the rest of the layers and adsorbed species of $TiCl_4$ and $AlEt_3$ were fully relaxed.

Data availability

The data that support the findings of this study are available from the corresponding author upon reasonable request.

Received: 25 May 2024; Accepted: 22 July 2024
Published online: 01 August 2024

References

1. Huang, J. & Rempel, G. L. Ziegler-Natta catalysts for olefin polymerization: Mechanistic insights from metallocene systems. *Prog. Polym. Sci.* **20**, 459–526. https://doi.org/10.1016/0079-6700(94)00039-5 (1995).
2. Kumawat, J. & Gupta, V. K. Fundamental aspects of heterogeneous Ziegler-Natta olefin polymerization catalysis: An experimental and computational overview. *Polym. Chem.* **11**, 6107–6128. https://doi.org/10.1039/D0PY00753F (2020).
3. D'Amore, M. *et al.* Surface investigation and morphological analysis of structurally disordered MgCl2 and MgCl2/TiCl4 Ziegler-Natta catalysts. *ACS Catal.* **6**, 5786–5796. https://doi.org/10.1021/acscatal.6b00871 (2016).
4. Pirinen, S., Jayaratne, K. C., Denifl, P. & Pakkanen, T. T. Ziegler-Natta catalysts supported on crystalline and amorphous MgCl2/THF complexes. *J. Mol. Catal. A Chem.* **395**, 434–439 (2014).
5. Sacchi, M. C., Tritto, I. & Locatelli, P. Stereochemical investigation of the effect of Lewis bases in heterogeneous Ziegler-Natta initiator systems. *Prog. Polym. Sci.* **16**, 331–360. https://doi.org/10.1016/0079-6700(91)90022-D (1991).
6. Tkachenko, O. P. *et al.* A Study of Ziegler-Natta propylene polymerization catalysts by spectroscopic methods. *Materials* **10**, 496 (2017).
7. Soares, J. B. P., Kim, J. D. & Rempel, G. L. Analysis and control of the molecular weight and chemical composition distributions of Polyolefins made with Metallocene and Ziegler–Natta catalysts. *Ind. Eng. Chem. Res.* **36**, 1144–1150. https://doi.org/10.1021/ie960479x (1997).
8. Zannetti, R., Marega, C., Marigo, A. & Martorana, A. Layer-lattices in Ziegler-Natta catalysts. *J. Polym. Sci. B Polym. Phys.* **26**, 2399–2412. https://doi.org/10.1002/polb.1988.090261202 (1988).
9. Hodgkin, D. C. The X-ray analysis of complicated molecules. *Science* **150**, 979–988. https://doi.org/10.1126/science.150.3699.979 (1965).
10. Böhm, L. L. High mileage Ziegler-catalysts: Excellent tools for polyethylene production. *Macromol. Symp.* **173**, 53–64. https://doi.org/10.1002/1521-3900(200108)173:1%3c53::AID-MASY53%3e3.0.CO;2-T (2001).
11. Böhm, L. L. The ethylene polymerization with Ziegler Catalysts: Fifty years after the discovery. *Angew. Chem. Int. Ed.* **42**, 5010–5030. https://doi.org/10.1002/anie.200300580 (2003).
12. Al-Arifi, A. S. N. Propylene polymerization using MgCl2/ethylbenzoate/TiCl4 catalyst: Determination of titanium oxidation states. *J. Appl. Polym. Sci.* **93**, 56–62. https://doi.org/10.1002/app.20378 (2004).
13. Fregonese, D., Mortara, S. & Bresadola, S. Ziegler-Natta MgCl2-supported catalysts: Relationship between titanium oxidation states distribution and activity in olefin polymerization. *J. Mol. Catal. A Chem.* **172**, 89–95. https://doi.org/10.1016/S1381-1169(01)00128-5 (2001).
14. Niu, Q., Zhang, J., Peng, W., Fan, Z. & He, A. Effect of alkylaluminium on the regio- and stereoselectivity in copolymerization of isoprene and butadiene using TiCl4/MgCl2 type Ziegler-Natta catalyst. *Mol. Catal.* **471**, 1–8. https://doi.org/10.1016/j.mcat.2019.04.009 (2019).

15. Pongchan, T., Praserthdam, P. & Jongsomjit, B. Gas-phase polymerization of ethylene over Ti-based Ziegler-Natta catalysts prepared from different magnesium sources. *Mater. Today Chem.* **18**, 100366. https://doi.org/10.1016/j.mtchem.2020.100366 (2020).
16. Jacobs, G. *et al.* Fischer-Tropsch synthesis: Support, loading, and promoter effects on the reducibility of cobalt catalysts. *Appl. Catal. A Gener.* **233**, 263–281. https://doi.org/10.1016/S0926-860X(02)00195-3 (2002).
17. Jiang, B. *et al.* Kinetics and mechanism of ethylene polymerization with TiCl4/MgCl2 model catalysts: Effects of titanium content. *J. Catal.* **360**, 57–65. https://doi.org/10.1016/j.jcat.2018.01.008 (2018).
18. Wada, T., Taniike, T., Kouzai, I., Takahashi, S. & Terano, M. Propylene polymerization performance of isolated and aggregated Ti species studied using a well-designed TiCl3/MgCl2 Ziegler-Natta model catalyst. *Macromol. Rapid Commun.* **30**, 887–891. https://doi.org/10.1002/marc.200900015 (2009).
19. Xiong, H.-F., Zhang, Y.-H., Li, J.-L. & Gu, Y.-Y. Effect of cobalt loading on reducibility, dispersion and crystallite size of Co/Al2O3 fischer-tropsch catalyst. *J. Cent. South Univ. Technol.* **11**, 414–418. https://doi.org/10.1007/s11771-004-0086-2 (2004).
20. Taniike, T., Wada, T., Kouzai, I., Takahashi, S. & Terano, M. Role of dispersion state of ti species in deactivation of MgCl2-supported Ziegler-Natta catalysts. *Macromol. Res.* **18**, 839–844. https://doi.org/10.1007/s13233-010-0914-1 (2010).
21. Taniike, T. & Terano, M. High-precision molecular modelling for Ziegler-Natta catalysts. *J. Jpn. Petrol. Inst.* **61**, 182–190. https://doi.org/10.1627/jpi.61.182 (2018).
22. Zorve, P. & Linnolahti, M. Adsorption of Titanium Tetrachloride on Magnesium Dichloride Clusters. *ACS Omega* **3**, 9921–9928. https://doi.org/10.1021/acsomega.8b01878 (2018).
23. Cheng, R.-H. *et al.* Adsorption of TiCl4 and electron donor on defective MgCl2 surfaces and propylene polymerization over Ziegler-Natta catalyst: A DFT study. *Chin. J. Polym. Sci.* **31**, 591–600. https://doi.org/10.1007/s10118-013-1252-5 (2013).
24. Redzic, E. *et al.* Heterogeneous Ziegler-Natta catalysts with various sizes of MgCl2 crystallites: Synthesis and characterization. *Iran. Polym. J.* **25**, 321–337. https://doi.org/10.1007/s13726-016-0424-x (2016).
25. Almeida, L. A. & MarquesdFV, M. Synthesis of a TiCl4 Ziegler-Natta catalyst supported on spherical MgCl2 nEtOH for the polymerization of ethylene and propylene. *Macromol. React. Eng.* **6**, 57–64. https://doi.org/10.1002/mren.201100049 (2012).
26. Bahri-Laleh, N. Interaction of different poisons with MgCl2/TiCl4 based Ziegler-Natta catalysts. *Appl. Surf. Sci.* **379**, 395–401. https://doi.org/10.1016/j.apsusc.2016.04.034 (2016).
27. Gnanakumar, E. S. *et al.* MgCl2·6CH3OH: A simple molecular adduct and its influence as a porous support for olefin polymerization. *ACS Catal.* **3**, 303–311. https://doi.org/10.1021/cs300730j (2013).
28. Taniike, T. & Terano, M. in *Polyolefins: 50 years after Ziegler and Natta I: Polyethylene and Polypropylene* (ed Walter Kaminsky) 81–97 (Springer Berlin Heidelberg, 2013).
29. Taniike, T. & Terano, M. Coadsorption and support-mediated interaction of Ti species with Ethyl Benzoate in MgCl2-supported heterogeneous Ziegler-Natta catalysts studied by density functional calculations. *Macromol. Rapid Commun.* **28**, 1918–1922. https://doi.org/10.1002/marc.200700363 (2007).
30. Gnanakumar, E. S. *et al.* 9-Fluorenemethanol: An internal electron donor to fine tune olefin polymerization activity. *Dalton Trans.* **43**, 9143–9151. https://doi.org/10.1039/C4DT00793J (2014).
31. Credendino, R. *et al.* Periodic DFT modeling of bulk and surface properties of MgCl2. *Phys. Chem. Chem. Phys.* **11**, 6525–6532. https://doi.org/10.1039/B905676A (2009).
32. Zorve, P. & Linnolahti, M. Catalytic reactions on magnesium dichloride clusters saturated by titanium tetrachloride. *Mol. Catal.* **499**, 111314. https://doi.org/10.1016/j.mcat.2020.111314 (2021).
33. Ludlum, D. B., Anderson, A. W. & Ashby, C. E. The polymerization of ethylene by lower valent compounds of titanium. *J. Am. Chem. Soc.* **80**, 1380–1384. https://doi.org/10.1021/ja01539a027 (1958).
34. Zhang, Z., Jiang, B.-Y., Zhang, B., Fu, Z.-S. & Fan, Z.-Q. Deactivation Effect Caused by Catalyst-Cocatalyst Pre-contact in Propylene Polymerization with MgCl2-supported Ziegler-Natta Catalyst. *Chin. J. Polyme. Sci.* **37**, 1023–1030. https://doi.org/10.1007/s10118-019-2319-8 (2019).
35. Credendino, R., Liguori, D., Fan, Z., Morini, G. & Cavallo, L. Toward a unified model explaining heterogeneous Ziegler-Natta catalysis. *ACS Catal.* **5**, 5431–5435. https://doi.org/10.1021/acscatal.5b01076 (2015).
36. D'Amore, M., Credendino, R., Budzelaar, P. H. M., Causá, M. & Busico, V. A periodic hybrid DFT approach (including dispersion) to MgCl2-supported Ziegler-Natta catalysts – 1: TiCl4 adsorption on MgCl2 crystal surfaces. *J. Catal.* **286**, 103–110. https://doi.org/10.1016/j.jcat.2011.10.018 (2012).
37. Gnanakumar, E. S. *et al.* MgCl2·6C6H11OH: A high mileage porous support for Ziegler-Natta catalyst. *J. Phys. Chem. C* **116**, 24115–24122. https://doi.org/10.1021/jp3074078 (2012).
38. Kresse, G. & Furthmüller, J. Efficiency of ab-initio total energy calculations for metals and semiconductors using a plane-wave basis set. *Comput. Mater. Sci.* **6**, 15–50. https://doi.org/10.1016/0927-0256(96)00008-0 (1996).
39. Kresse, G. & Furthmüller, J. Efficient iterative schemes for ab initio total-energy calculations using a plane-wave basis set. *Phys. Rev. B* **54**, 11169–11186. https://doi.org/10.1103/PhysRevB.54.11169 (1996).
40. Kresse, G. & Hafner, J. Ab initio molecular dynamics for liquid metals. *Phys. Rev. B* **47**, 558–561. https://doi.org/10.1103/PhysRevB.47.558 (1993).
41. Kresse, G. & Hafner, J. Ab initio molecular-dynamics simulation of the liquid-metal–amorphous-semiconductor transition in germanium. *Phys. Rev. B* **49**, 14251–14269. https://doi.org/10.1103/PhysRevB.49.14251 (1994).
42. Perdew, J. P., Burke, K. & Ernzerhof, M. Generalized gradient approximation made simple. *Phys. Rev. Lett.* **77**, 3865–3868. https://doi.org/10.1103/PhysRevLett.77.3865 (1996).
43. Teter, M. P., Payne, M. C. & Allan, D. C. Solution of Schr"odinger's equation for large systems. *Phys. Rev. B* **40**, 12255–12263. https://doi.org/10.1103/PhysRevB.40.12255 (1989).
44. Grimme, S., Antony, J., Ehrlich, S. & Krieg, H. A consistent and accurate ab initio parametrization of density functional dispersion correction (DFT-D) for the 94 elements H-Pu. *J. Chem. Phys.* https://doi.org/10.1063/1.3382344 (2010).
45. Monkhorst, H. J. & Pack, J. D. Special points for Brillouin-zone integrations. *Phys. Rev. B* **13**, 5188–5192. https://doi.org/10.1103/PhysRevB.13.5188 (1976).
46. Momma, K. & Izumi, F. VESTA 3 for three-dimensional visualization of crystal, volumetric and morphology data. *J. Appl. Crystallogr.* **44**, 1272–1276. https://doi.org/10.1107/S0021889811038970 (2011).
47. Henkelman, G., Arnaldsson, A. & Jónsson, H. A fast and robust algorithm for Bader decomposition of charge density. *Comput. Mater. Sci.* **36**, 354–360. https://doi.org/10.1016/j.commatsci.2005.04.010 (2006).
48. Sanville, E., Kenny, S. D., Smith, R. & Henkelman, G. Improved grid-based algorithm for Bader charge allocation. *J. Comput. Chem.* **28**, 899–908. https://doi.org/10.1002/jcc.20575 (2007).
49. Yu, M. & Trinkle, D. R. Accurate and efficient algorithm for Bader charge integration. *J. Chem. Phys.* https://doi.org/10.1063/1.3553716 (2011).
50. Tang, W., Sanville, E. & Henkelman, G. A grid-based Bader analysis algorithm without lattice bias. *J. Phys. Condens. Matter* **21**, 084204. https://doi.org/10.1088/0953-8984/21/8/084204 (2009).

Acknowledgements

All authors highly acknowledged that this research was supported by the Second Century Fund (C2F). Also, the following funding are acknowledged: (1) Thailand Science Research and Innovation Fund Chulalongkorn

University (FF2567), (2) National Science and Technology Development Agency, Thailand, (3) the NSRF via the Program Management Unit for Human Resources & Institutional Development, Research and Innovation (PMU-B) (Grant No. B16F640143), (4) Hub of Knowledge funding, National Research Council of Thailand (NRCT), and (5) the Mid-Career Research Grant 2024, National Research Council of Thailand (NRCT). We also thank computational resources from NSTDA Supercomputer Center (ThaiSC), and CECC-HCU.

Author contributions
T.S., M.R., S.P. conceived the computational simulations. T.S., N.K., and C.N. performed the computational simulations. P.S. and N.B. prepared the catalysts, did the characterizations, and harvested the results in the experimental section. T.S., P.S., C.N., N.K., M.R., P.K., J.S., N.B., P.P., and S.P. performed data analyses, wrote the paper, reviewed and revised the manuscript.

Funding
Chulalongkorn University,the Second Century Fund (C2F),the Second Century Fund (C2F),the Second Century Fund (C2F),the Second Century Fund (C2F),the Second Century Fund (C2F),Graduate School,Chulalongkorn University,Ministry of Higher Education,Science,Research and Innovation,Thailand,B16F640143 and B13F6654,B16F640143 and B13F6654,National Research Council of Thailand,Hub of Knowledge funding,Hub of Knowledge funding.

Competing interests
The authors declare no competing interests.

Additional information
Supplementary Information The online version contains supplementary material available at https://doi.org/10.1038/s41598-024-68289-8.

Correspondence and requests for materials should be addressed to S.P.